dimensionless flat-bed widths that are greater than or equal to 5.0, and are thus called 'wide' channels. Figure 5.8 plots the upper limits of δ_{cr}^{*} ranges, against the μ values for which these ranges are valid. The behavior shown in this plot is well represented by the equation

$$d_{cr\max}^{*} = 0.878m^{-0.079} \qquad \text{for } 0.4 \le m \le 1.0 \qquad (24)$$

where

$d_{cr\max}^{*}$ = upper limit of δ_{cr}^{*} range for a given value of μ

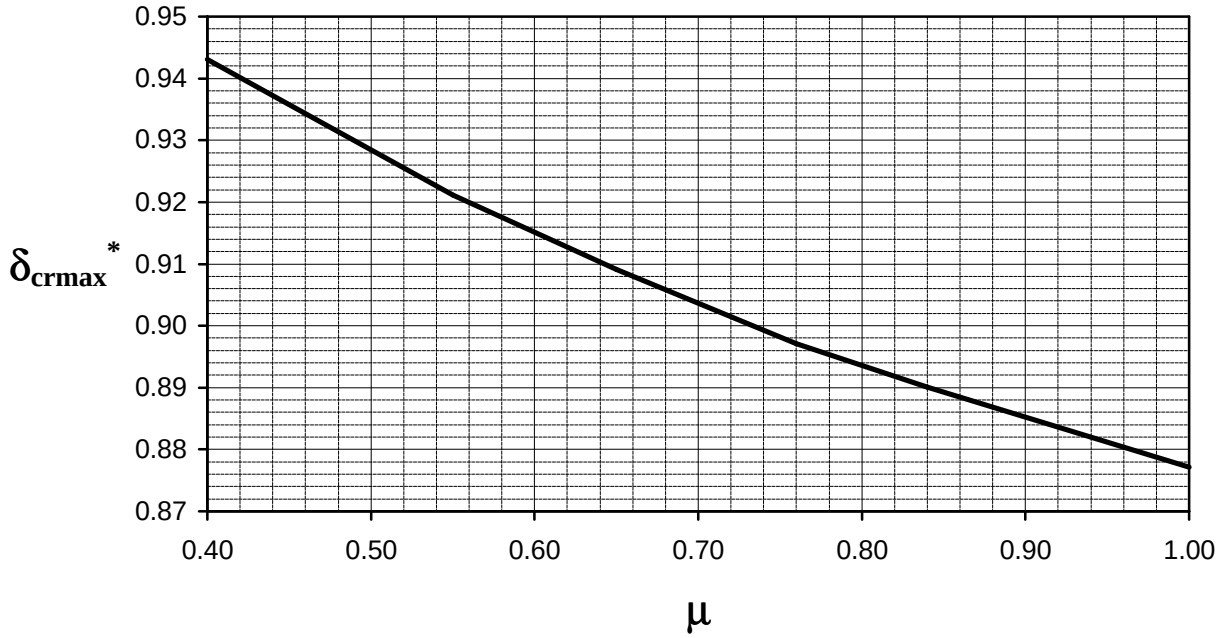

Figure 5.8. Variation of $d_{cr\max}^{*}$ with μ

Table 5.1 lists the values of the lower and upper limits of δ_{cr}^{*} ranges that correspond to a given value of μ.

Table 5.1. Limits of δ_{cr}^{*} ranges that are valid for a given value of μ.

μ	δ_{crmin}^{*}	δ_{crmax}^{*}
0.40	0.930	0.943
0.55	0.900	0.921
0.65	0.885	0.909
0.76	0.870	0.897
0.84	0.860	0.890
1.00	0.845	0.877

The dimensionless bank width of the channel was observed to be highly dependent on μ and δ_{cr}^*, while remaining practically insensitive to changes in β (for most purposes, β can be assumed to have a value of 0.85). Furthermore, it was found that for a given value of μ, B_s^* can be expressed as a function of δ_{cr}^* alone. The following equation form can be used to determine values of B_s^* that closely approximate the values predicted by the numerical model.

$$B_s^* / 2 = c_2 d_{cr}^{*\,2} + c_1 d_{cr}^* + c_0 \tag{25}$$

The coefficients c_2, c_1, and c_0 in equation 25 are given in Table 5.2. These vary depending on the value of μ, as can be seen in Figures 5.9a to 5.9c. The following equations adequately describe the behavoir shown in the figures, and can be used to determine these coefficients:

$$c_2 = 129.133 m^{-1.973} \tag{26}$$

$$c_1 = -229.736 m^{-2.043} \tag{27}$$

$$c_0 = 104.425 m^{-2.094} \tag{28}$$

Table 5.2. Coefficients of the equation $B_s^* / 2 = c_2 d_{cr}^{*\,2} + c_1 d_{cr}^* + c_0$, for different μ values.

μ	c_2	c_1	c_0
0.4	798.735	-1516.07	723.847
0.55	415.051	-770.105	360.751
0.65	292.761	-536.762	249.186
0.76	217.369	-394.1	181.493
0.84	195.91	-352.021	160.834
1.0	126.08	-224.78	102.646

As seen earlier, Figure 5.5a plots B_s^* as a function of δ_{cr}^*, for different μ values. As long as the design engineer knows what values of μ and δ_{cr}^* to use, either Equation 25 or Figure 5.5a can be used to determine the corresponding value of B_s^*.

It can be seen in Figure 5.5a that for a given value of δ_{cr}^*, B_s^* decreases as μ increases. This is consistent with the idea that banks composed of material having a higher μ value can afford steeper lateral slopes, which in turn results in shorter bank widths. On the other hand, for a given value of μ, an increase in δ_{cr}^* is accompanied by a decrease in B_s^*. Recall that a higher value of δ_{cr}^* results in less lateral diffusion of momentum toward the channel banks. This smaller momentum transfer in turn causes the stress surfeit in the bank region to be less. Thus, the banks can maintain steeper lateral slopes, and consequently, have shorter widths.

Once B_s^* is known, the water discharge for the bank region Q_{bank} can be determined.

$$Q_{bank} = \alpha_1 \bar{u} A_{bank} \tag{29}$$

where

α_1 = correction factor

$\bar{u}$ = mean velocity based on mean depth $\bar{D}$ of the bank region

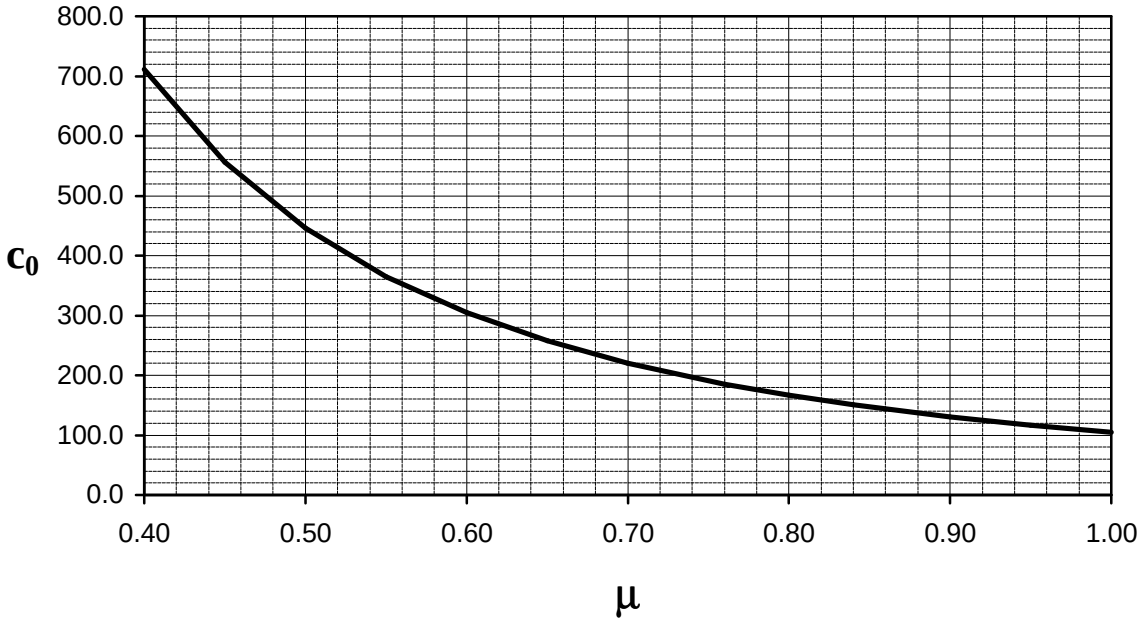

Figure 5.9a. Variation of coefficient c_0 with μ

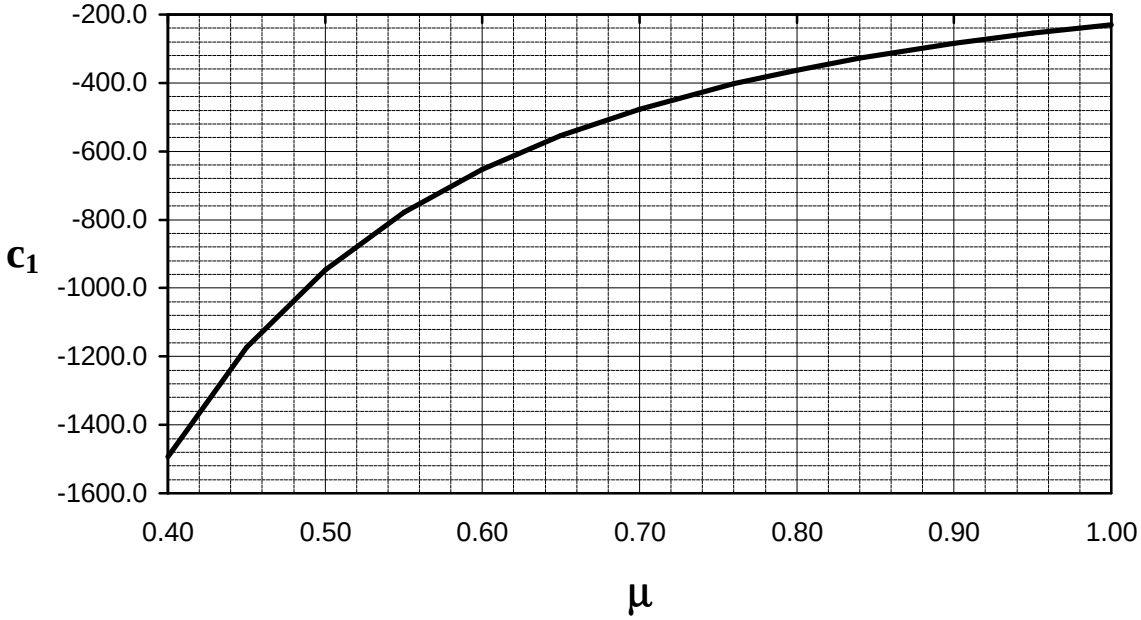

Figure 5.9b. Variation of coefficient c_1 with μ

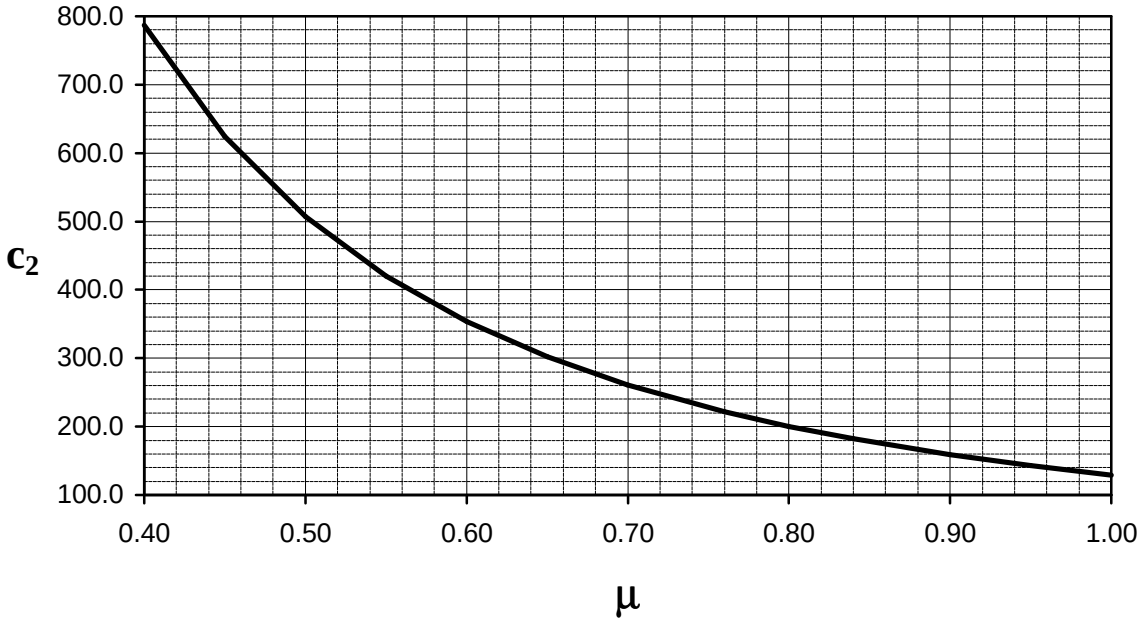

Figure 5.9c. Variation of coefficient c_2 with μ

$\overline{D} = A_{bank}/B_s$

A_{bank} = cross-sectional area of the bank region

A correction factor α_1 has to be applied to Equation 29. If $\alpha_1 = 1.0$, the formula yields bank discharge values that are consistently smaller than those predicted by the numerical model. By comparing the values of discharge predicted by the formula and the model, it was found that α_1 varies from 1.145 to 1.185 for $0.4 \le m \le 1.0$. To simplify things, assuming an average value of 1.165 for all μ values within the aforementioned range, gives reasonable bank discharge values. However, using the appropriate α_1 value for a given value of μ allows Equation 29 to give values of bank discharge that are within 2% of the corresponding model values. This is shown in Table 5.3. The variation of α_1 with μ is shown in Figure 5.10a, and given by the equation

$$\alpha_1 = 0.066\mu + 1.119 \qquad (30)$$

The model also showed a fairly consistent relation between the cross-sectional area A_{bank} of the bank region, and the bank width.

$$A_{bank} = a_2 B_s^* D_c^2 \qquad (31)$$

The coefficient α_2 is dependent on μ, and may be determined using Figure 5.10b or the following equation:

$$\alpha_2 = 0.0297\mu + 0.6422 \qquad (32)$$

Figure 5.10c plots the relationship between dimensionless bank cross-sectional area $A_{bank}^* (= A_{bank} / D_c^2)$ and B_s^*, for different values of μ.

In reality, for a given value of μ, α_2 varies slightly over the corresponding δ_{cr}^* range. In fact, a more accurate formula for A_{bank} would be

Table 5.3. Comparison of Q_{bank} values obtained from numerical model and from design equations.

	$B_s^*/2$	α_1	α_2	Q_{bank}^*	D_c (m)	equation Q_{bank} (m^3/s)	numerical model Q_{bank} (m^3/s)	% difference
$\mu = 0.40$	4.72	1.146	0.654	14.30	2.96	108.57	109.43	0.78
	4.59	1.146	0.654	13.91	2.93	102.74	103.73	0.95
	4.50	1.146	0.654	13.64	2.92	99.85	99.60	-0.25
	4.48	1.146	0.654	13.58	2.92	99.37	98.87	-0.50
	4.47	1.146	0.654	13.55	2.92	99.14	98.17	-1.00
	4.47	1.146	0.654	13.53	2.91	98.15	97.49	-0.68
$\mu = 0.55$	3.85	1.155	0.659	11.90	3.06	98.86	100.63	1.76
	3.73	1.155	0.659	11.54	3.04	94.17	94.53	0.39
	3.66	1.155	0.659	11.31	3.02	90.68	90.57	-0.13
	3.60	1.155	0.659	11.13	3.01	88.46	87.38	-1.23
	3.57	1.155	0.659	11.03	3.00	86.89	85.70	-1.40
	3.55	1.155	0.659	10.97	2.99	85.64	84.64	-1.18
	3.55	1.155	0.659	10.96	2.99	85.59	84.14	-1.73
$\mu = 0.65$	3.45	1.162	0.661	10.77	3.11	93.50	95.12	1.70
	3.36	1.162	0.661	10.49	3.09	89.50	90.04	0.60
	3.29	1.162	0.661	10.27	3.07	86.13	86.45	0.37
	3.24	1.162	0.661	10.12	3.06	84.08	83.53	-0.67
	3.20	1.162	0.661	9.99	3.04	81.60	80.98	-0.77
	3.19	1.162	0.661	9.96	3.04	81.35	80.51	-1.04
	3.18	1.162	0.661	9.93	3.03	80.38	80.04	-0.42
	3.18	1.162	0.661	9.92	3.03	80.28	79.59	-0.86
	3.17	1.162	0.661	9.89	3.03	80.10	79.14	-1.21

Table 5.3. Comparison of Q_{bank} values obtained from numerical model and from design equations (continued).

	$B_s^*/2$	α_1	α_2	Q_{bank}^*	D_c (m)	equation Q_{bank} (m^3/s)	numerical model Q_{bank} (m^3/s)	% difference
$\mu = 0.76$	3.16	1.169	0.665	10.01	3.16	90.77	92.29	1.65
	3.07	1.169	0.665	9.73	3.14	86.75	87.53	0.88
	3.01	1.169	0.665	9.54	3.12	83.64	84.09	0.53
	2.97	1.169	0.665	9.41	3.11	81.80	81.28	-0.63
	2.93	1.169	0.665	9.28	3.09	79.26	78.84	-0.54
	2.89	1.169	0.665	9.16	3.07	76.89	76.65	-0.30
	2.89	1.169	0.665	9.14	3.07	76.75	76.24	-0.67
	2.88	1.169	0.665	9.14	3.07	76.67	75.83	-1.11
$\mu = 0.84$	3.01	1.175	0.667	9.62	3.20	90.13	91.12	1.10
	2.97	1.175	0.667	9.49	3.19	88.30	89.35	1.17
	2.93	1.175	0.667	9.39	3.18	86.84	87.54	0.80
	2.92	1.175	0.667	9.34	3.18	86.14	86.81	0.77
	2.86	1.175	0.667	9.16	3.16	83.20	83.33	0.16
	2.82	1.175	0.667	9.02	3.14	80.67	80.51	-0.20
	2.78	1.175	0.667	8.90	3.13	78.41	78.22	-0.23
	2.77	1.175	0.667	8.86	3.12	77.56	77.19	-0.48
	2.76	1.175	0.667	8.82	3.11	76.75	76.36	-0.51
	2.75	1.175	0.667	8.80	3.11	76.31	75.97	-0.44
	2.74	1.175	0.667	8.78	3.10	75.94	75.54	-0.54
	2.73	1.175	0.667	8.74	3.10	75.17	74.81	-0.48
	2.73	1.175	0.667	8.73	3.10	74.77	74.33	-0.58
	2.722	1.175	0.667	8.71	3.09	74.43	74.00	-0.58

Table 5.3. Comparison of Q_{bank} values obtained from numerical model and from design equations (continued).

	$B_s^*/2$	α_1	α_2	Q_{bank}^*	D_c (m)	equation Q_{bank} (m^3/s)	numerical model Q_{bank} (m^3/s)	% difference
$\mu = 1.00$	2.74	1.185	0.672	8.95	3.25	87.90	88.70	0.90
	2.67	1.185	0.672	8.71	3.24	84.64	84.55	-0.11
	2.63	1.185	0.672	8.57	3.22	81.88	81.44	-0.55
	2.59	1.185	0.672	8.45	3.20	79.42	78.82	-0.76
	2.55	1.185	0.672	8.34	3.18	77.02	76.54	-0.63
	2.53	1.185	0.672	8.26	3.16	75.02	74.47	-0.73
	2.50	1.185	0.672	8.16	3.14	72.85	72.59	-0.36
	2.49	1.185	0.672	8.13	3.14	72.59	72.23	-0.50
	2.49	1.185	0.672	8.11	3.14	72.44	71.87	-0.79

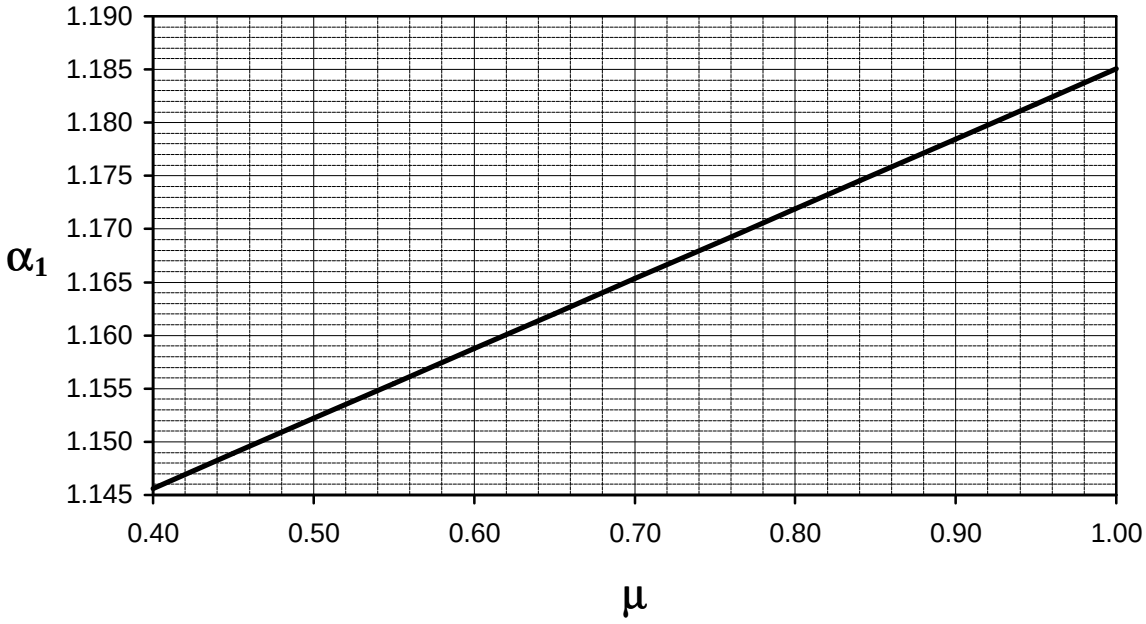

Figure 5.10a. Variation of coefficient α_1 with μ

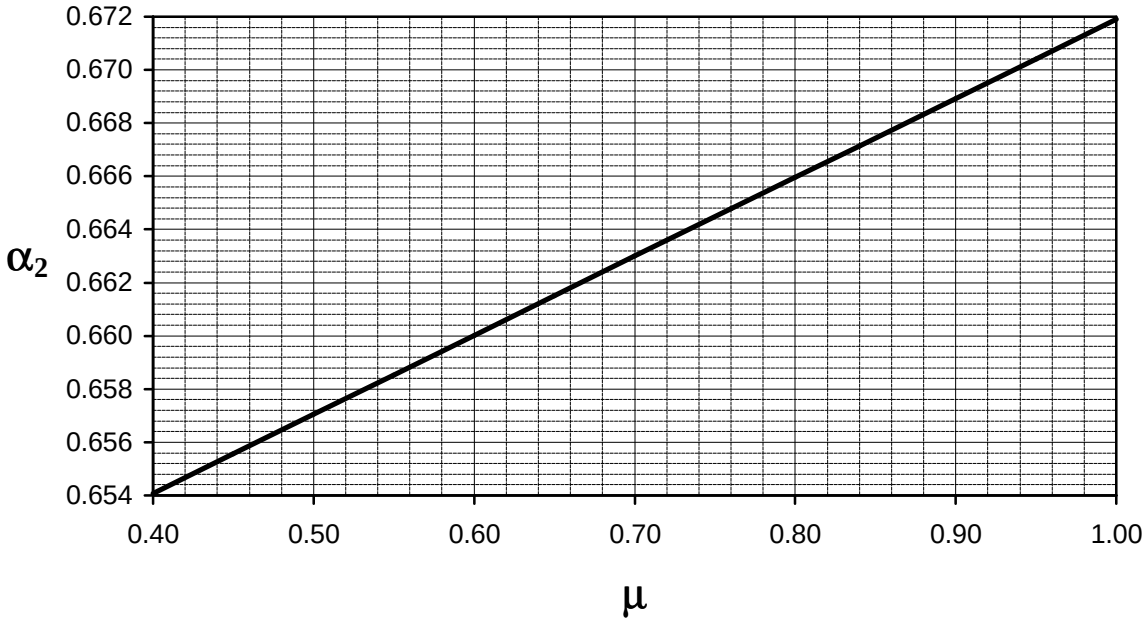

Figure 5.10b. Variation of coefficient α_2 with μ

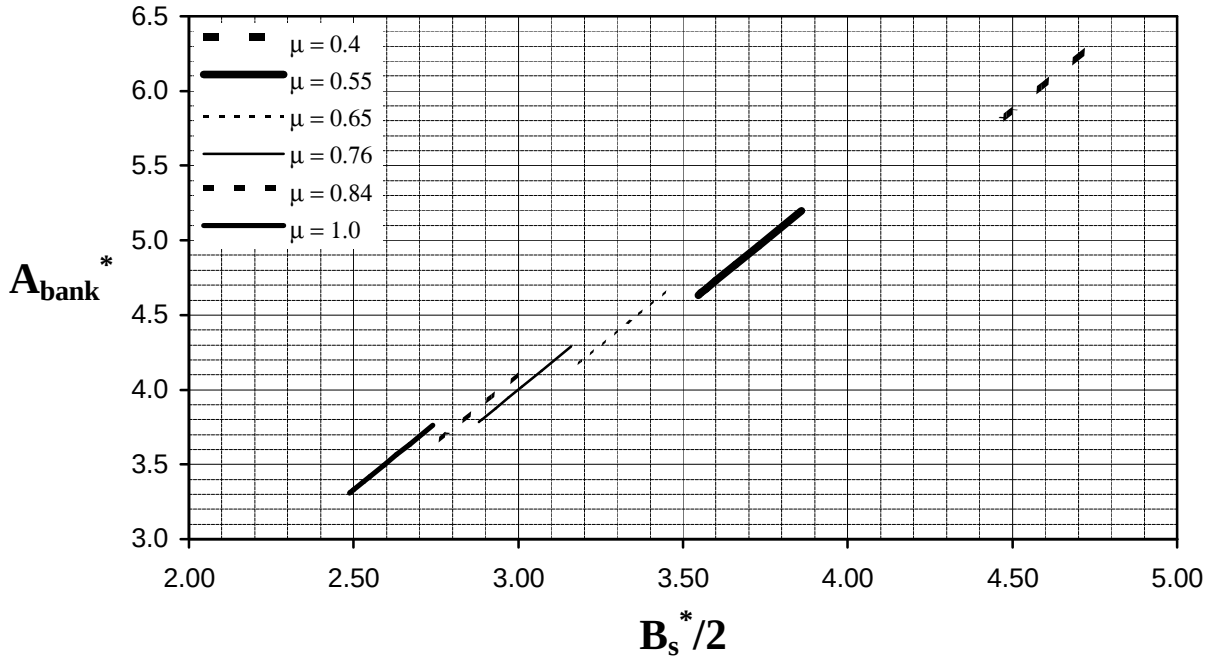

Figure 5.10c. Variation of dimensionless bank cross-sectional area A^*_{bank} with dimensionless half-bank width $B^*_s / 2$

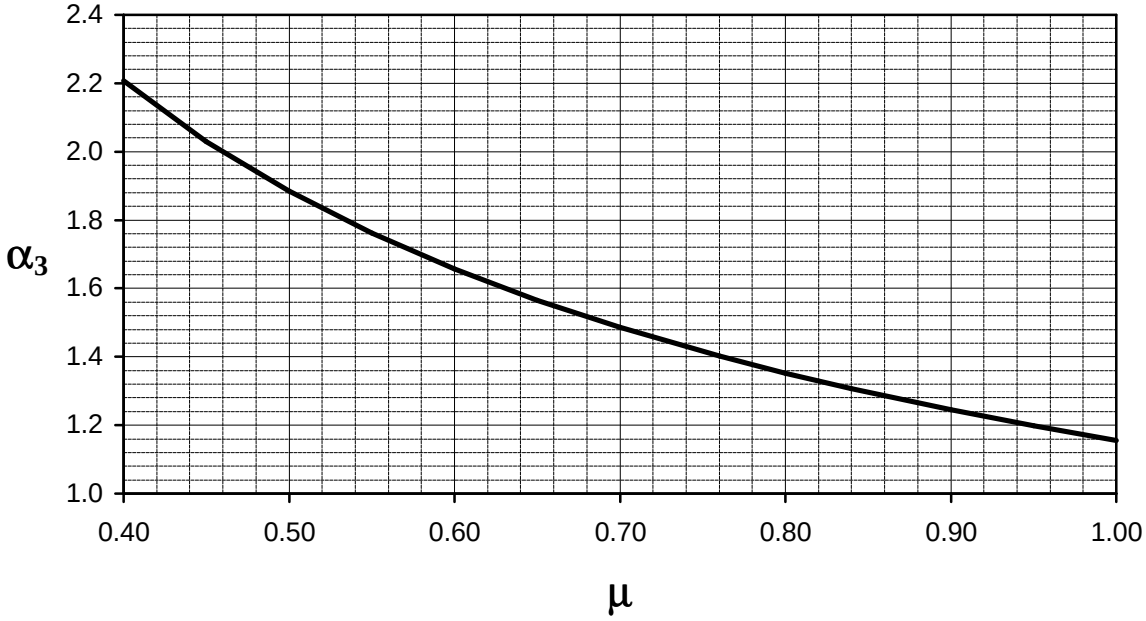

Figure 5.11. Variation of coefficient α_3 with μ

$$A_{bank} = \left(0.9B_s^* - a_3\right)D_c^2 \quad (33)$$

where

$\alpha_3 = 1.1551\mu^{-0.7063}$; shown in Figure 5.11 (34)

The difference between the values predicted by Equations 31 and 33 is demonstrated in Figures 5.12a to 5.12f. However, Equation 31 yields values of bank cross-sectional area that are still within 2% of those predicted by the model. Moreover, the compact form of Equation 31 makes it easy to develop a simple yet reliable expression for Q_{bank}. Examination of Equation 31 shows that the mean depth $\overline{D}$ for the bank region can be reasonably approximated as $\alpha_2 D_c$. This is used in Equation 35 to calculate the mean velocity over the bank region.

$$\overline{u} = 2.5\sqrt{gS\overline{D}}\ln\left(\frac{11\overline{D}}{k}\right) \quad (35)$$

This expression is similar to the one used by Keulegan (1938). Substituting Equations 31 and 35 in Equation 29 results in the formula for discharge in the bank region.

$$Q_{bank} = 2.5a_1 a_2^{1.5}\sqrt{gSD_c^5}B_s^*\ln\left(\frac{11a_2}{k^*}\right) \quad (36)$$

where

$k^* = d_{90}/D_c$.

The bank discharge values predicted by Equation 36 are in good agreement with the values generated by the numerical model (Figures 5.13a to 5.13f). Equation 36 can be modified into an expression for dimensionless bank discharge, which is plotted in Figures 5.14a to 5.14g for $\alpha_1 = 1.165$:

$$Q_{bank}^* = \frac{Q_{bank}}{\sqrt{gSD_c^5}\ln\left(\frac{11a_2}{k^*}\right)} = 2.5a_1 a_2^{1.5}B_s^* \quad (37)$$

The coefficients a_1, α_2, as well as α_3, used to calculate A_{bank}^* and Q_{bank} are shown in Table 5.4 for different values of μ.

Once the bank discharge has been calculated, it can be subtracted from the total water discharge to get the discharge over the flat-bed region Q_f. The equation for discharge over the flat-bed region is derived using the expression

$$Q_f = \int u dA_{bed} \quad (38)$$

where

$u = 2.5\sqrt{gSD_c d^*(y^*)}\ln\left(\frac{11}{k^*}\right)$; mean velocity over the flat-bed region

$dA_{bed} = D_c^2\, dy^*$

Since the channel cross-section is symmetrical about its center, the water discharge over the entire flat-bed region can be calculated by integrating over half the flat-bed width, and then taking twice the result. This leads to the expression

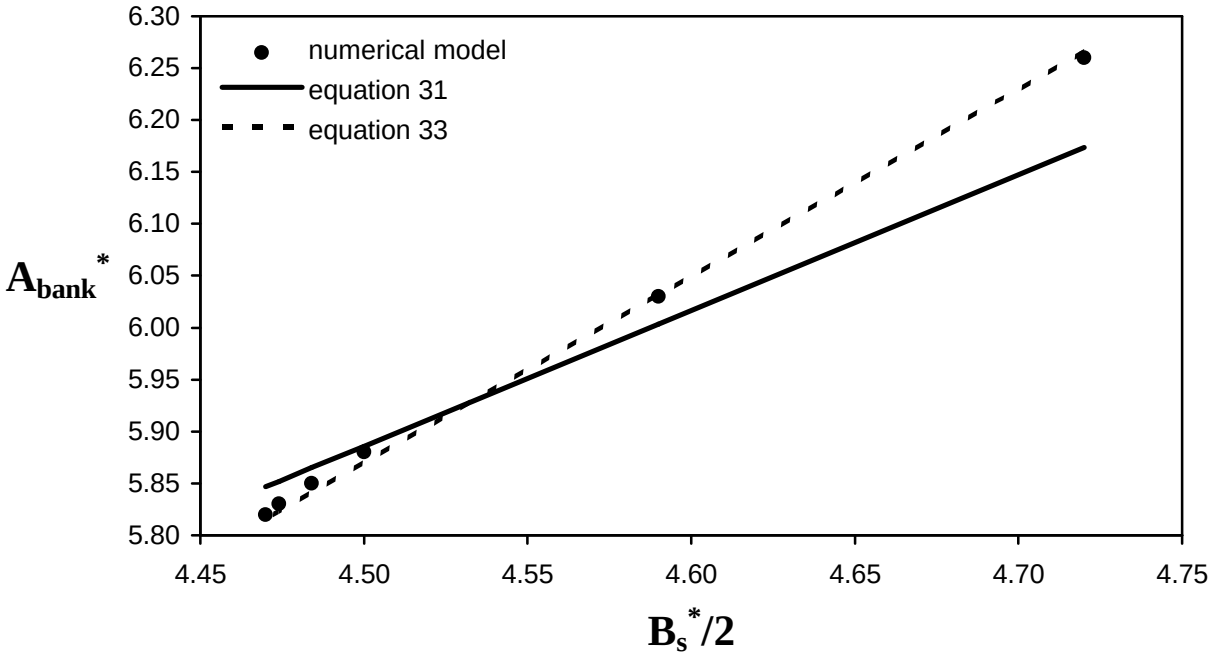

Figure 5.12a. Comparison of equations for determining A^*_{bank}; μ = 0.4

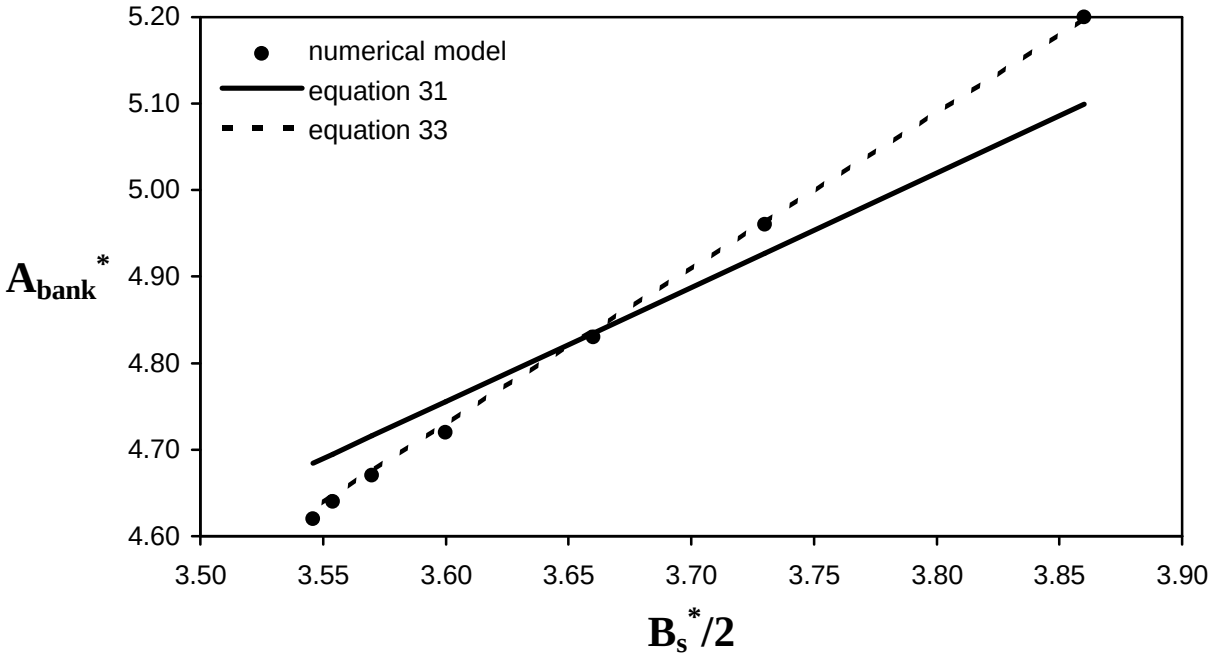

Figure 5.12b. Comparison of equations for determining A^*_{bank}; μ = 0.55

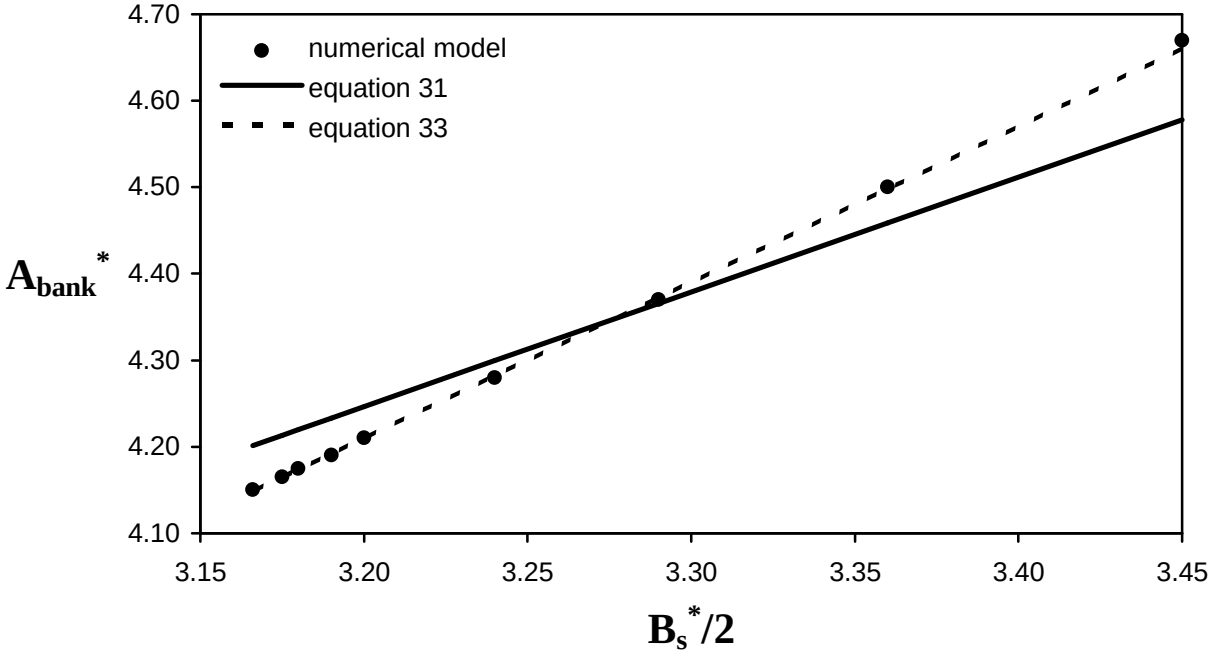

Figure 5.12c. Comparison of equations for determining A^*_{bank}; μ = 0.65

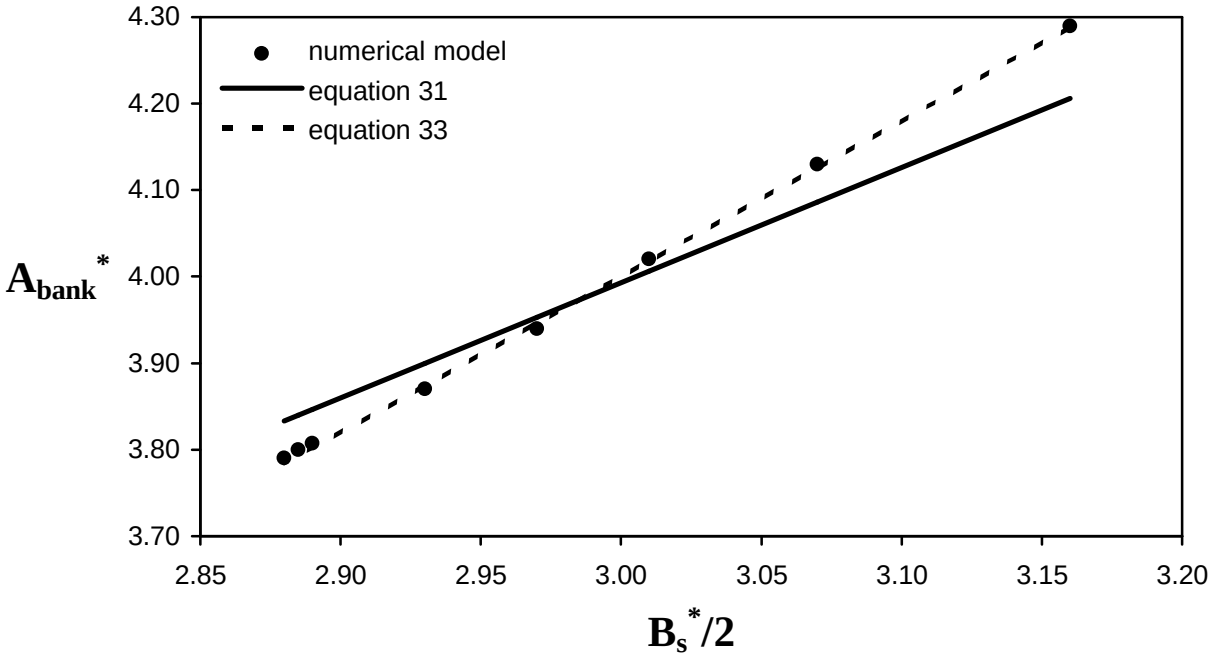

Figure 5.12d. Comparison of equations for determining A^*_{bank}; μ = 0.76

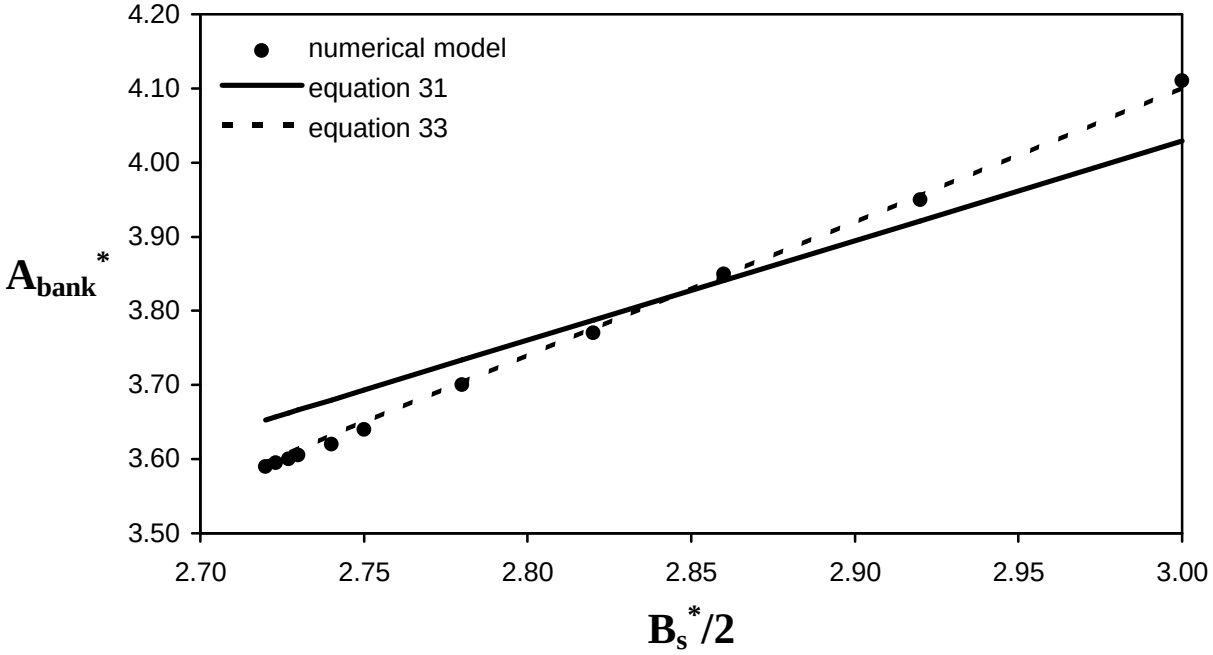

Figure 5.12e Comparison of equations for determining A^*_{bank} ; μ = 0.84

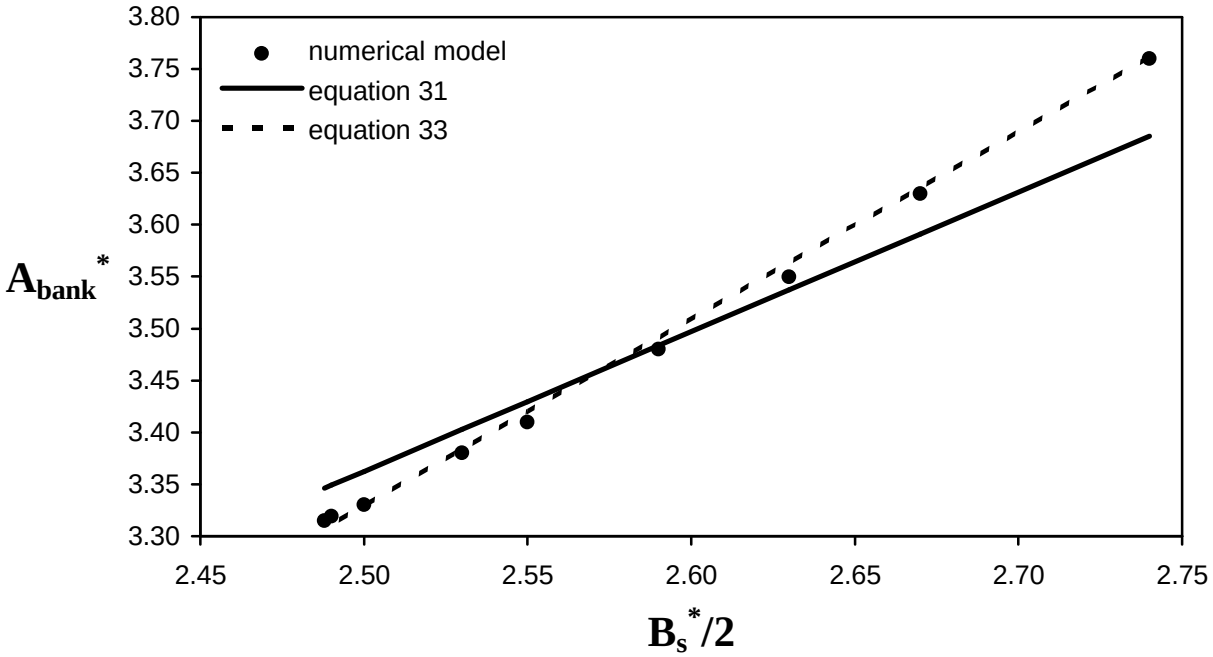

Figure 5.12f. Comparison of equations for determining A^*_{bank} ; μ = 1.0

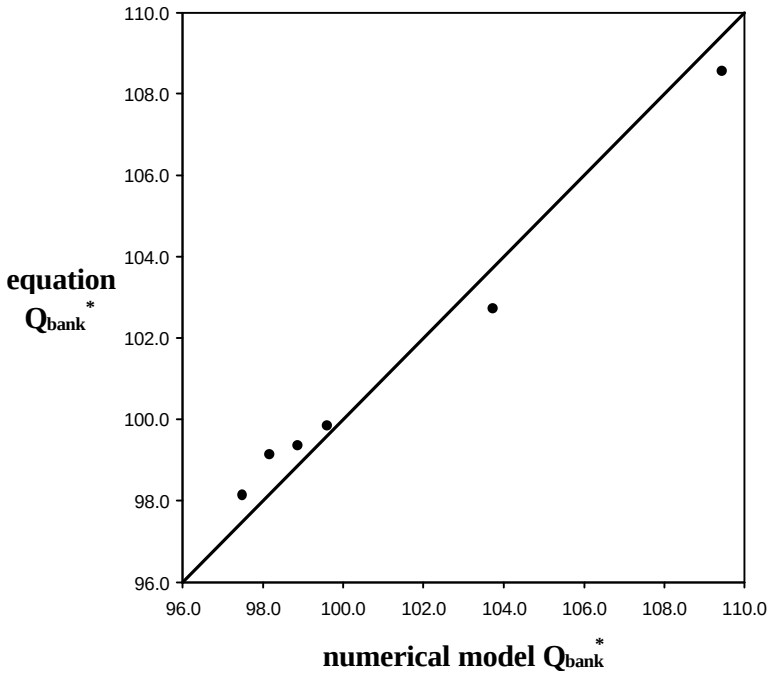

Figure 5.13a. Comparison of Q_{bank} values predicted by numerical model and equation; $\mu = 0.4$

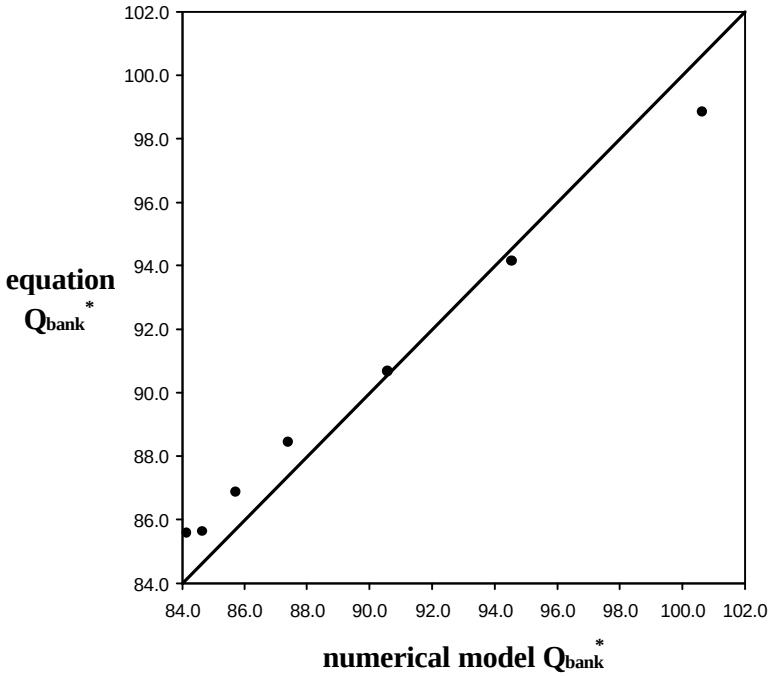

Figure 5.13b. Comparison of Q_{bank} values predicted by numerical model and equation; $\mu = 0.55$

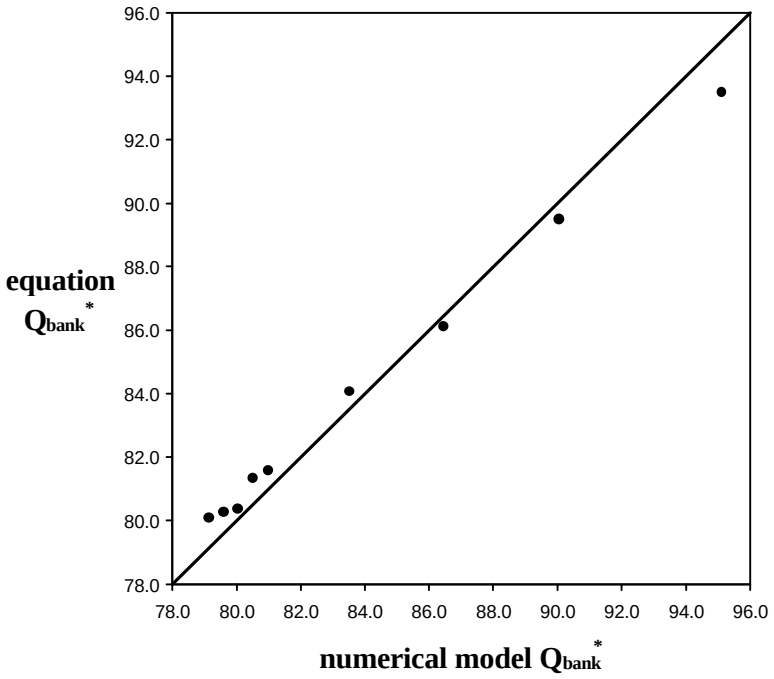

Figure 5.13c. Comparison of Q_{bank} values predicted by numerical model and equation; $\mu = 0.65$

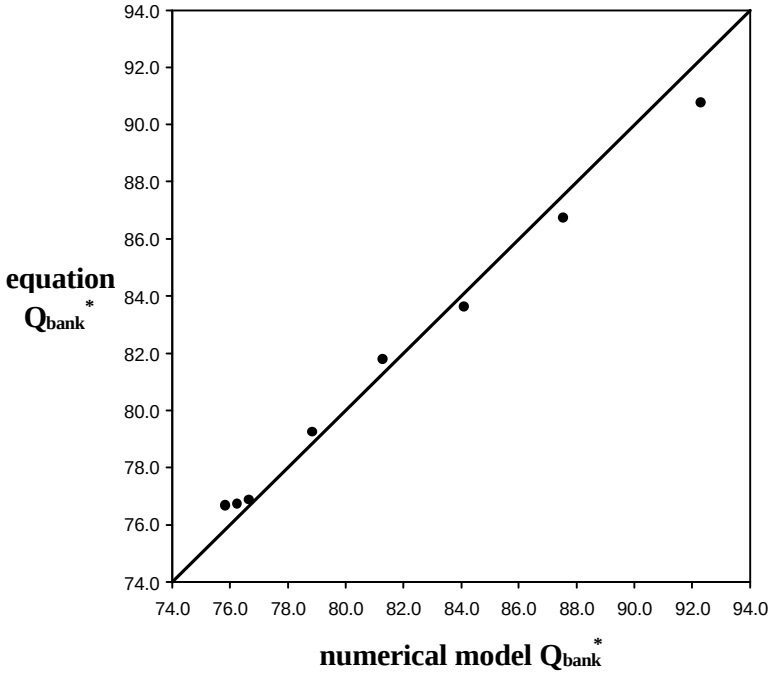

Figure 5.13d. Comparison of Q_{bank} values predicted by numerical model and equation; $\mu = 0.76$

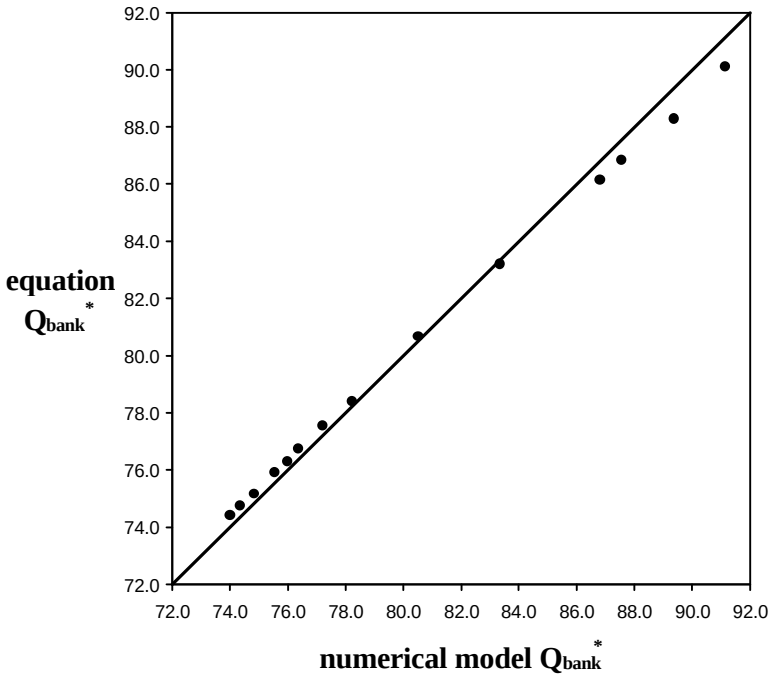

Figure 5.13e. Comparison of Q_{bank} values predicted by numerical model and equation; $\mu = 0.84$

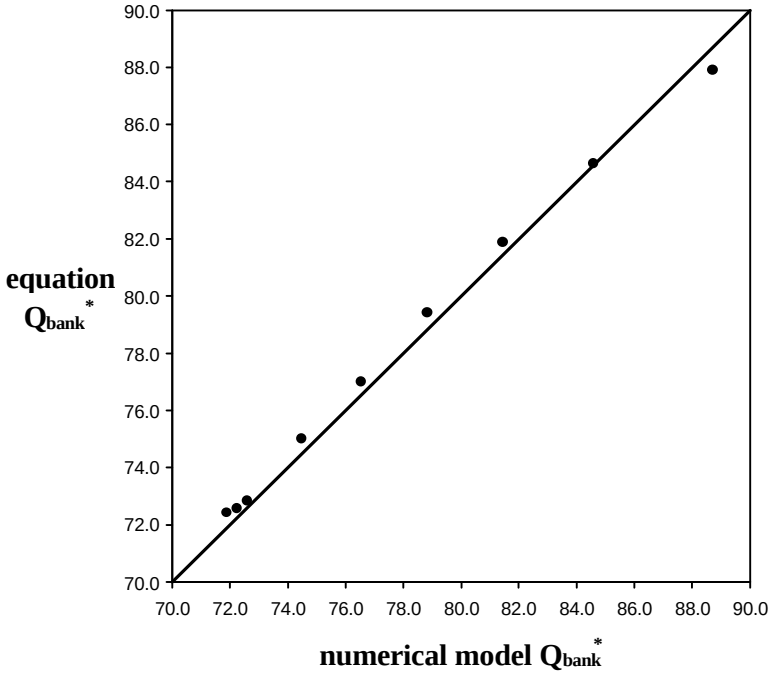

Figure 5.13f. Comparison of Q_{bank} values predicted by numerical model and equation; $\mu = 1.0$

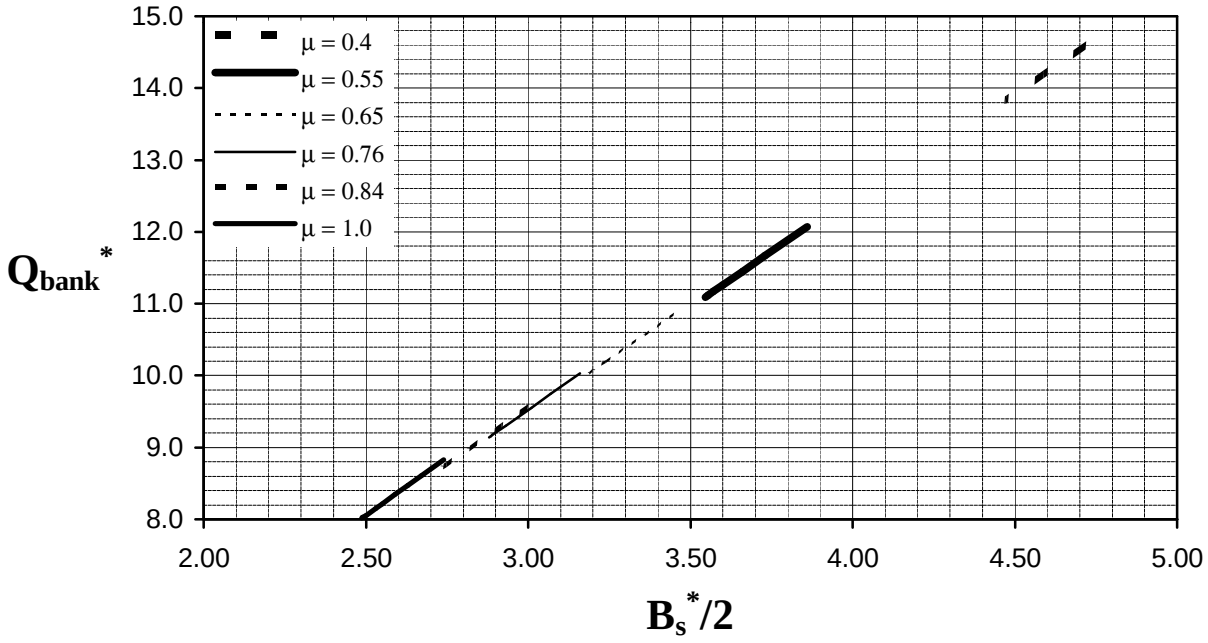

Figure 5.14a. Variation of dimensionless bank discharge Q^*_{bank} with dimensionless half-bank width $B^*_s / 2$, for different values of μ

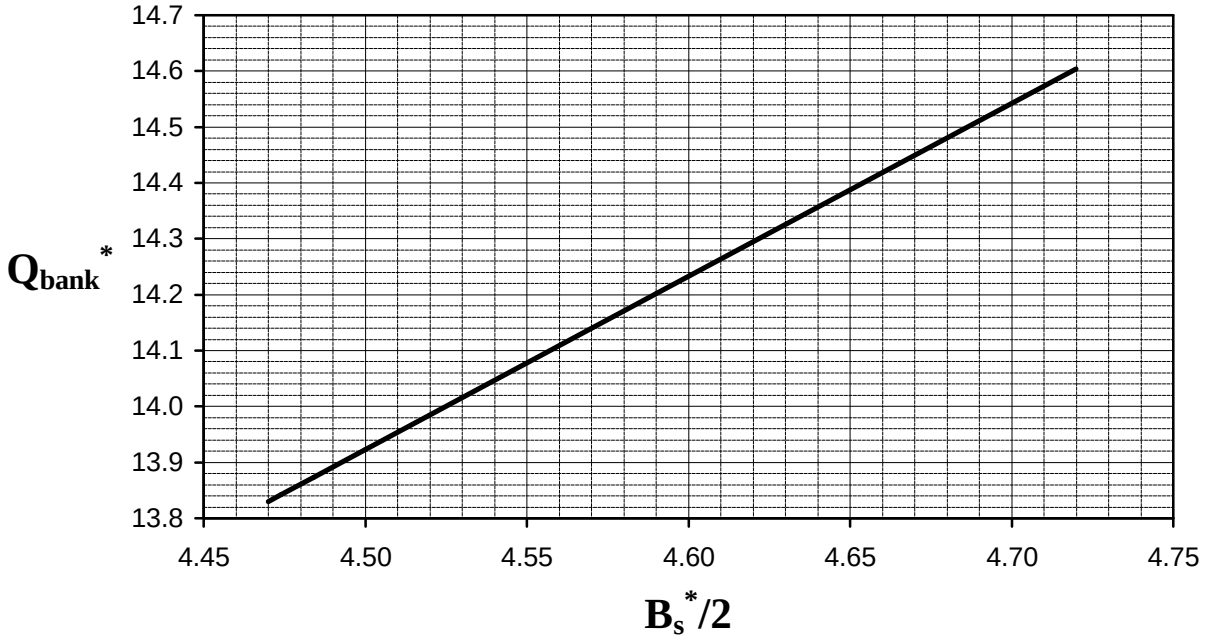

Figure 5.14b. Variation of dimensionless bank discharge Q^*_{bank} with dimensionless half-bank width $B^*_s / 2$; μ = 0.4

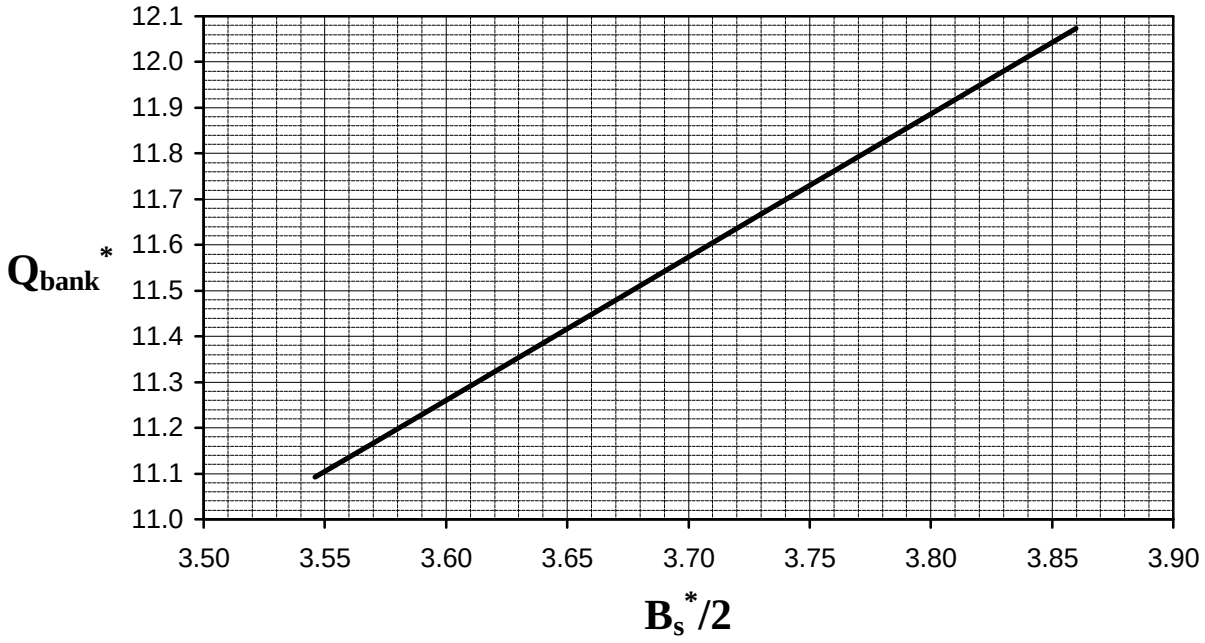

Figure 5.14c. Variation of dimensionless bank discharge Q^*_{bank} with dimensionless half-bank width $B^*_s / 2$; $\mu = 0.55$

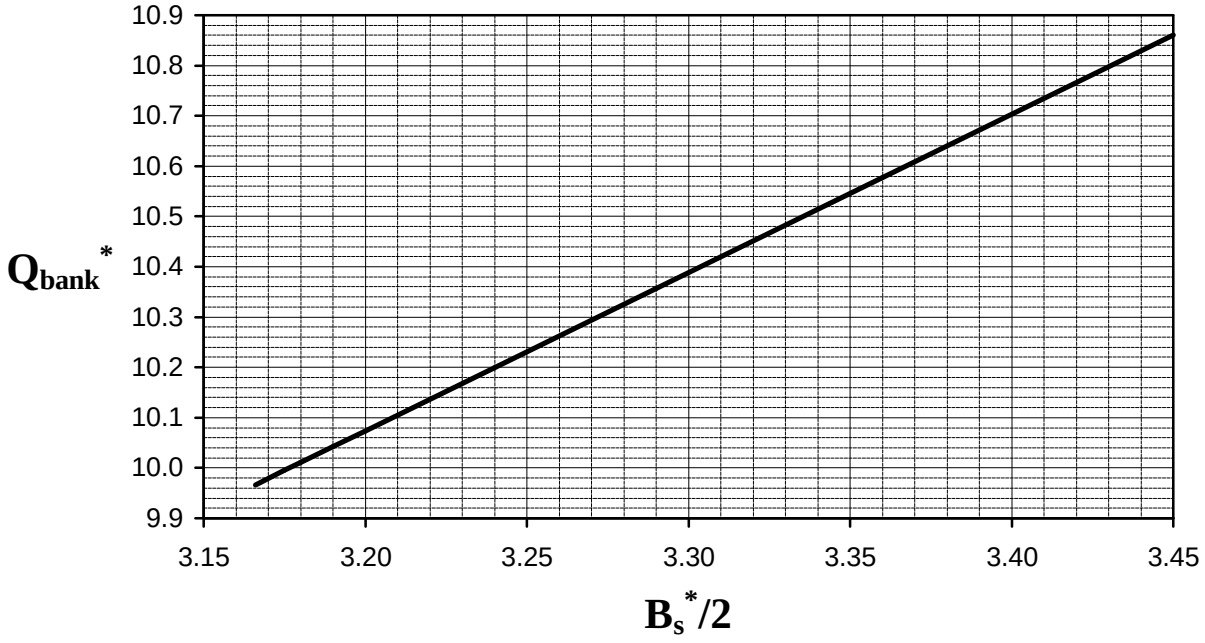

Figure 5.14d. Variation of dimensionless bank discharge Q^*_{bank} with dimensionless half-bank width $B^*_s / 2$; $\mu = 0.65$

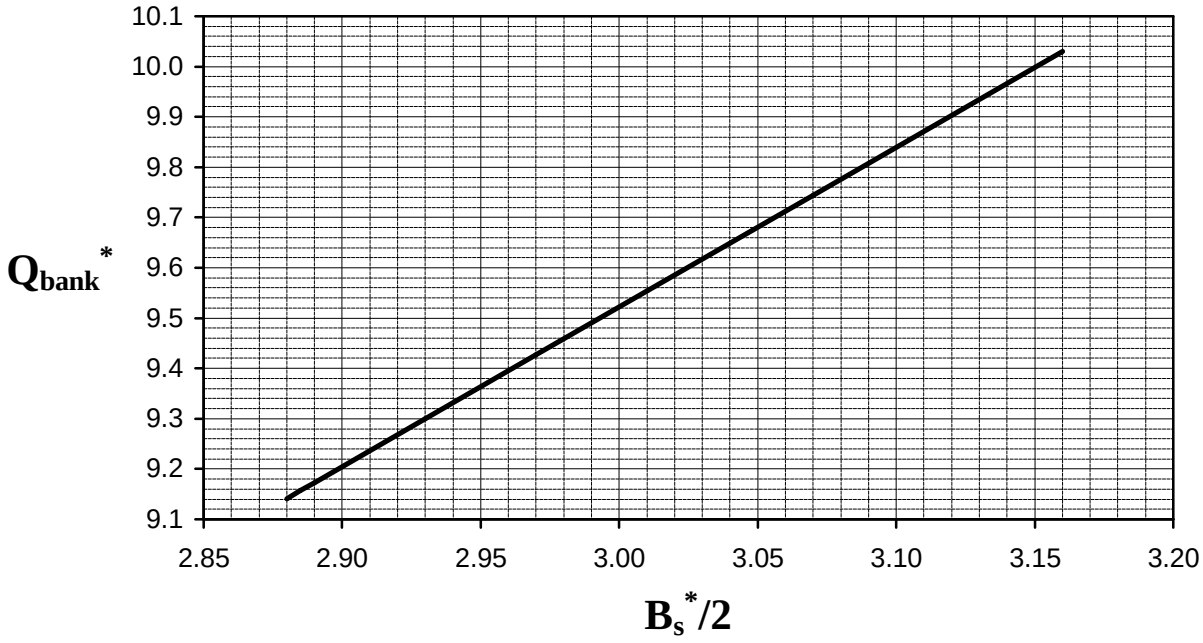

Figure 5.14e. Variation of dimensionless bank discharge Q^*_{bank} with dimensionless half-bank width $B^*_s / 2$; $\mu = 0.76$

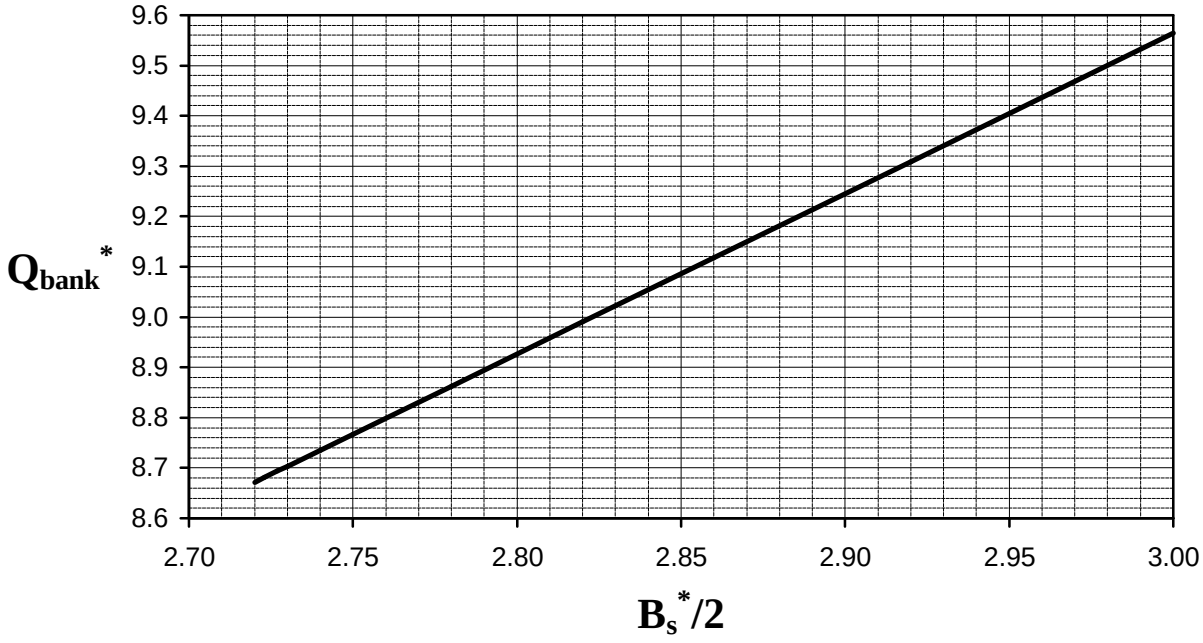

Figure 5.14f. Variation of dimensionless bank discharge Q^*_{bank} with dimensionless half-bank width $B^*_s / 2$; $\mu = 0.84$

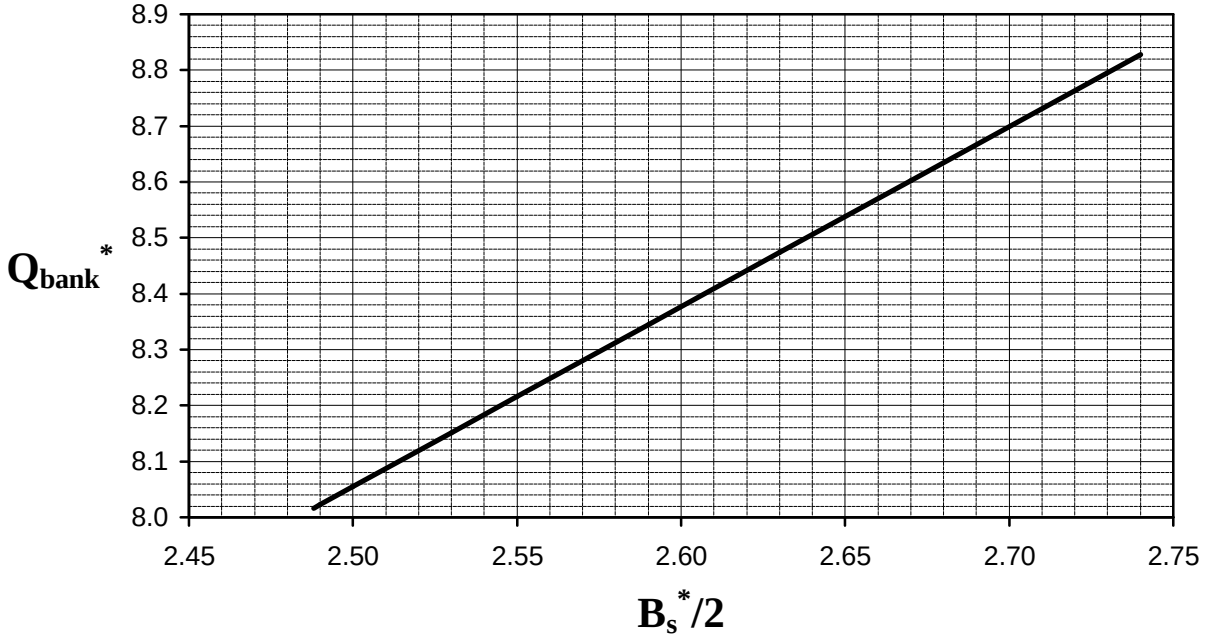

Figure 5.14g. Variation of dimensionless bank discharge Q^*_{bank} with dimensionless half-bank width $B^*_s / 2$; $\mu = 1.0$

Table 5.4. Coefficients of equations used for calculating Q_{bank} and $A_{bank}{}^*$.

μ	α_1	α_2	α_3
0.40	1.146	0.654	2.23
0.55	1.155	0.659	1.75
0.65	1.162	0.661	1.55
0.76	1.169	0.665	1.40
0.84	1.175	0.667	1.30
1.00	1.185	0.672	1.17

$$Q_f = 2\int_0^{\frac{B_f^*}{2}} 2.5\sqrt{gS\delta^*(y^*)D_c^5}\,\ln\left(\frac{11}{k^*}\right)dy^* \qquad (39)$$

Recall that equation 14 gives the stress-depth $\delta^*(y^*)$ at any point on the flat-bed region. Substituting equation 14 in 39 and then integrating yields the equation for water discharge over the flat-bed region.

$$Q_f = 5\sqrt{gSD_c^5}\,\ln\left(\frac{11}{k^*}\right)\left[\frac{B_f^*}{2} + \sqrt{\psi_o}\left(\delta_{cr}^* - 1\right)\tanh\left(\frac{B_f^*}{2\sqrt{\psi_o}}\right)\right] \qquad (40)$$

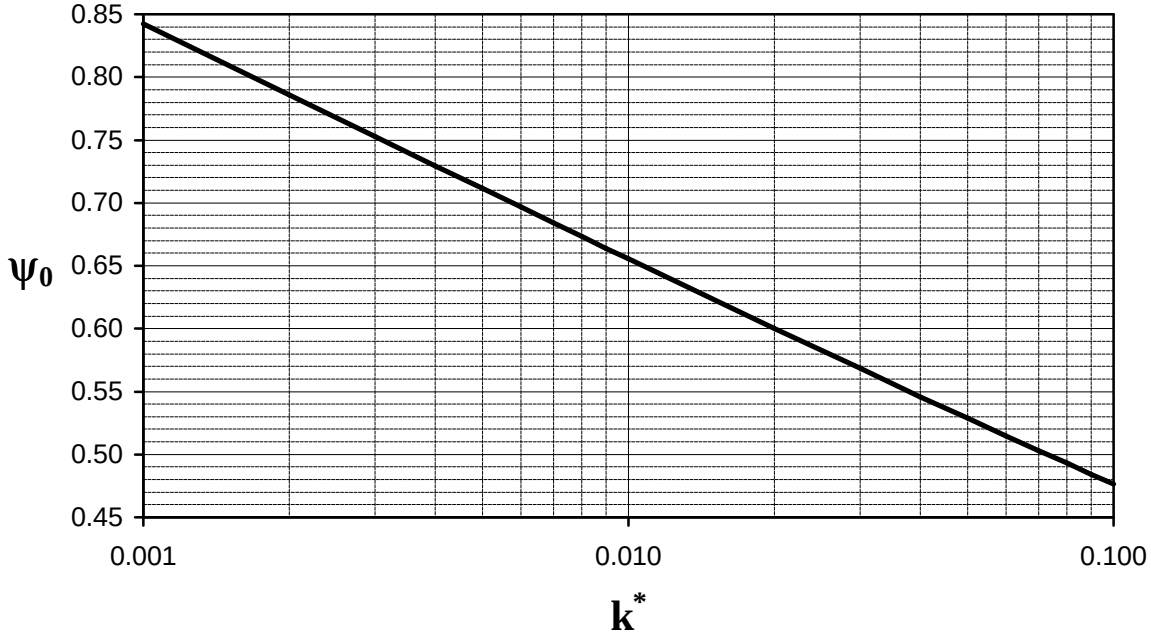

Figure 5.15. Variation of ψ_0 with k^*

The value of ψ_0 in Equation 40 is a function of k^*. It may be graphically determined using Figure 5.15.

Equation 40 can be solved by trial and error to find the dimensionless flat-bed width B_f^*. For wide channels, $\delta_{cr}^* = d_{cr\max}^*$ for a given value of μ, and Equation 40 is sufficient to determine B_f^*. For narrow channels however, B_f^* is unique for a given value of δ_{cr}^* and μ, as shown in Figure 5.6a. Equation 40 must therefore be used in conjunction with Figure 5.6a to determine B_f^* for a narrow channel.

Once B_f^* is known, the top channel width can be calculated.

$$B = D_c\left(B_f^* + B_s^*\right) \tag{41}$$

The bank profile can be generated using an equation of the form

$$D^* = a_3 d^{*3} + a_2 d^{*2} + a_1 d^* + a_0 \tag{42}$$

where

$D^* = D/D_c$ = dimensionless vertical channel depth

D = vertical channel depth

$d^* = d/D_c$ = dimensionless lateral distance from junction point

$d = y - B_f/2$ = lateral distance from junction point

The coefficients of Equation 42 vary with δ_{cr}^* and μ, and are shown in Table 5.5. For combinations of δ_{cr}^* and μ not shown in the table, adequate coefficients can be obtained by means of interpolation.

Table 5.5. Coefficients of bank profile equation $D^* = a_3 d^{*3} + a_2 d^{*2} + a_1 d^* + a_0$, for different values of μ and d^*_{cr}.

	d^*_{cr}	a_3	a_2	a_1	a_0
μ = 0.4	0.93	---	-.0411	-.0135	+1.0001
	0.935	---	-.0412	-.0236	+1.0004
	0.94	---	-.0412	-.0307	+1.0008
	0.945	---	-.0413	-.0342	+1.0009
μ = 0.55	0.9	-0.0029	-0.0503	-0.018	+1.0003
	0.905	-0.0027	-0.0527	-0.0299	+1.0006
	0.91	-0.0025	-0.0547	-0.0366	+1.0008
	0.915	-0.0022	-0.0565	-0.0416	+1.001
	0.921	-0.0019	-0.0586	-0.0463	+1.0011
μ = 0.65	0.885	-0.006	-0.0543	-0.0278	+1.0006
	0.895	-0.0054	-0.06	-0.0444	+1.001
	0.905	-0.0048	-0.0647	-0.0529	+1.0013
	0.909	-0.0045	-0.0665	-0.0556	+1.0041
μ = 0.76	0.87	-0.0105	-0.0544	-0.0365	+1.0009
	0.88	-0.0101	-0.061	-0.0531	+1.0014
	0.89	-0.0095	-0.0662	-0.0621	+1.0017
	0.897	-0.009	-0.0701	-0.0662	+1.0018
μ = 0.84	0.86	-0.0146	-0.0516	-0.0418	+1.0011
	0.87	-0.0143	-0.059	-0.0594	+1.0016
	0.88	-0.0141	-0.0634	-0.0697	+1.002
	0.89	-0.013	-0.0708	-0.0742	+1.0021
μ = 1.0	0.845	-0.0233	-0.0466	-0.0571	+1.0016
	0.855	-0.0237	-0.0531	-0.0738	+1.0022
	0.865	-0.0236	-0.0589	-0.0828	+1.0025
	0.875	-0.023	-0.0656	-0.0884	+1.0028
	0.878	-0.0226	-0.0683	-0.0892	+1.0028

Table 5.6. Dimensionless parameters for defining optimal stable channels.

	δ_{cr}^*	A_{bank}^*	$B_s^*/2$	B_f^*	B^*
$\mu = 0.40$	0.930	6.26	4.72	0.49	9.93
	0.935	6.03	4.59	1.00	10.18
	0.940	5.88	4.50	1.85	10.85
	0.941	5.85	4.48	2.17	11.14
	0.942	5.83	4.47	2.70	11.65
	0.943	5.81	4.47	5.00	13.94
$\mu = 0.55$	0.900	5.20	3.86	0.25	7.97
	0.905	4.96	3.74	0.63	8.11
	0.910	4.83	3.66	1.01	8.33
	0.915	4.72	3.60	1.52	8.72
	0.918	4.67	3.57	2.05	9.19
	0.920	4.64	3.55	2.77	9.88
	0.921	4.62	3.55	5.00	12.09
$\mu = 0.65$	0.885	4.67	3.45	0.32	7.22
	0.89	4.48	3.36	0.63	7.35
	0.895	4.37	3.29	0.95	7.53
	0.900	4.28	3.24	1.34	7.82
	0.905	4.20	3.20	1.99	8.38
	0.906	4.19	3.19	2.21	8.59
	0.907	4.18	3.18	2.52	8.88
	0.908	4.16	3.18	3.01	9.36
	0.909	4.15	3.17	5.00	11.33
$\mu = 0.76$	0.870	4.29	3.16	0.31	6.63
	0.875	4.13	3.07	0.59	6.73
	0.880	4.02	3.01	0.86	6.88
	0.885	3.94	2.97	1.18	7.12
	0.890	3.87	2.93	1.61	7.47
	0.895	3.81	2.89	2.49	8.27
	0.896	3.80	2.89	2.89	8.66
	0.897	3.79	2.88	5.00	10.76

Table 5.6. Dimensionless parameters for defining optimal stable channels (continued).

	δ_{cr}^*	A_{bank}^*	$B_s^*/2$	B_f^*	B^*
$\mu = 0.84$	0.860	4.11	3.00	0.28	6.28
	0.865	3.95	2.92	0.55	6.39
	0.870	3.85	2.86	0.79	6.51
	0.875	3.77	2.82	1.07	6.71
	0.880	3.70	2.78	1.42	6.98
	0.885	3.64	2.75	1.97	7.47
	0.886	3.63	2.74	2.14	7.62
	0.888	3.61	2.73	2.66	8.12
	0.889	3.60	2.727	3.13	8.58
	0.890	3.60	2.723	5.00	10.45
$\mu = 1.00$	0.845	3.76	2.74	0.34	5.82
	0.850	3.64	2.67	0.57	5.91
	0.855	3.55	2.63	0.79	6.05
	0.860	3.48	2.59	1.03	6.21
	0.865	3.42	2.55	1.32	6.42
	0.870	3.37	2.53	1.75	6.81
	0.875	3.33	2.50	2.59	7.59
	0.876	3.32	2.49	2.96	7.94
	0.877	3.31	2.49	5.00	9.98

Table 5.6 summarizes, for different combinations of δ_{cr}^* and μ, the values of the dimensionless parameters that define the geometry of optimal stable channels. It should be reiterated that these values apply to narrow channels. The values of A_{bank}^* and $B_s^*/2$ corresponding to $d_{cr\max}^*$ for a given value of μ, apply to wide channels as well. However, the values of B_f^* and B^* still have to be determined using Equations 40 and 41 respectively.

The emphasis of this work is to determine the significant dimensions and bank shape of an optimal stable channel. However, recall that one of the major differences between an optimal stable channel and a threshold channel, is the former's ability to transport bedload over its flat-bed region. The design of such a channel would thus be incomplete without consideration of this bedload transport. Although a specific sediment relation is incorporated in the model for the purpose of illustration, it does not mean that this is the equation to use in all cases. No sediment transport relation is endorsed here, since there is no relation among the many available, that can be considered universally suitable. The design engineer must therefore choose a bedload relation that he deems appropriate for his particular case.